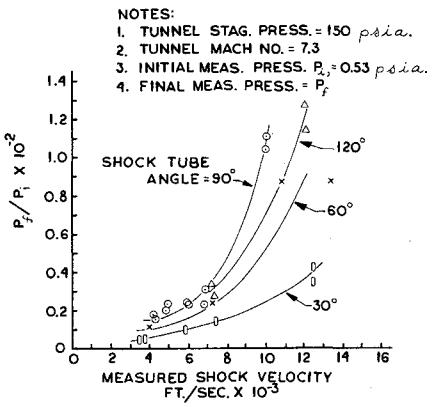

Fig. 4 Variation of model pressure ratio with shock velocity.

until the shock wave intersected the instrumentation. At intersection, a step change in pressure was observed. As would be expected, the pressure ratio increases with increasing shock velocity (Fig. 4). The pressure ratio varies from a maximum with the 90° shock tube to a minimum with the 30° tube. The variation is attributed to the attitude of the transducers relative to the advancing shock front and to variations in distance from the shock tube exit to the model.

It is concluded that the technique described in this paper provides a feasible method for simulating the interaction of a blast wave with a hypersonic body. It is also feasible to measure pressure-time histories on the body.

References

[1] Pierce, D., "Simulation of blast waves in a supersonic wind tunnel," Royal Aircraft Establishment TN AERO 2665 (January 1960).

[2] Thomas, R. E. and Lee, J. D., "The Ohio State University 12-inch hypersonic wind tunnel system," The Ohio State Univ. Rept. TN (ALOSU), pp. 559–562 (July 1959).

[3] Wilson, M. R. and Hienmenz, R. J., "Light source for high-speed photography," Research Trends Cornell Aeronautical Lab. Rept. Vol. VII (1959).

[4] Bitondo, D., Glass, I. I., and Patterson, G. N., "One dimensional theory of absorption and amplification of a plane shock wave by a gaseous layer," Univ. of Toronto Institute of Aerophysics Rept. 5, pp. 17–21 (June 1950).

Uniformly Loaded Plates of Regular Polygonal Shape

A. W. Leissa,* C. C. Lo,† and F. W. Niedenfuhr*
The Ohio State University, Columbus, Ohio

In a previous note Niedenfuhr and Leissa[1] used the point-matching method to determine torsional stresses and rotations of bars having regular polygonal cross sections. The present note summarizes results obtained in applying the method to the bending of uniformly loaded plates of regular polygonal shape with sides either clamped or simply supported.

The differential equation of equilibrium to be solved is

$$D\nabla^4 w = q_0 \tag{1}$$

Received November 2, 1965. The results contained in this note are a partial product of research supported by the U. S. Air Force under Contract No. AF33(657)8772, monitored by G. E. Maddux, ASRMDS-22, Wright Patterson Air Force Base.

* Professor, Department of Engineering Mechanics. Associate Fellow Member AIAA.

† Research Associate, Department of Engineering Mechanics.

Table 1 Deflections and moments; clamped edges

No. of sides, m	wD/q_0a^4 at $r = 0$	M/q_0a^2 at $r = 0$	M_x/q_0a^2 at $r = a, \theta = 0$
3	0.02414	0.09812	−0.2372
4	0.02024	0.09162	−0.2053
5	0.01861	0.08832	−0.1886
6	0.01774	0.08640	−0.1780
7	0.01722	0.08519	−0.1705
8	0.01687	0.08436	−0.1650
9	0.01663	0.08377	−0.1607
10	0.01645	0.08334	−0.1573
∞	0.01562	0.08125	−0.1250

where D is the flexural rigidity, ∇^4 is the biharmonic differential operator, w is the transverse deflection, and q_0 is the uniform transverse loading. An exact solution to Eq. (1) will be taken in polar coordinates as

$$w = \sum_{n=0}^{N} (A_n r^n + B_n r^{n+2}) \cos n\theta + \frac{q_0 r^4}{64D} \tag{2}$$

where the coefficients A_n and B_n are to be determined from the boundary conditions and the upper limit of summation N is determined by the accuracy of solution desired from the point matching process.

Typical plate geometry is exemplified by Fig. 1, wherein the special case of a hexagonal boundary is shown. The plate centroid is used as coordinate origin and θ is measured from a symmetry axis bisecting a side. The plate dimension is measured by denoting the radius of the inscribed circle as "a."

Taking advantage of the manifold symmetry present, the summation index n is taken successively as $0, m, 2m, 3m, \ldots$, where m is the number of sides for a particular regular polygon. The boundary conditions for all problems were applied at nine equally spaced points (including midpoints and vertices) in one sector subtended by the angle π/m as shown in Fig. 1. By symmetry considerations then, these boundary conditions are enforced in all $2m$ sectors of the polygon.

Clamped edge conditions were obtained by choosing $N = 8m$ and requiring the deflection and its normal derivative to be zero at the nine points. Solution of the resulting 18 simultaneous equations determines the coefficients A_n and B_n. Bending moments are evaluated by proper combination of second derivatives of deflection. The problem formulation, solution, and evaluation were accomplished automatically by means of a general-purpose computer program and significant results for $m = 3, 4, \ldots 10$ are presented in Table 1.

The accuracy of these solutions may be judged by two criteria: 1) the maximum deviation from exact boundary conditions between points matched, and 2) the rate of convergence of solutions as the number of boundary points used is changed. In Table 1, the maximum deviation from zero deflection along the boundary occurs in the case of the triangle

Table 2 Deflections, slopes, and moments; simply supported edges

No. of sides, m	wD/q_0a^4 at $r = 0$	M/q_0a^2 at $r = 0$	$D(\partial w/\partial x)/q_0a^3$ at $r = a, \theta = 0$
3	0.0833	0.217	−0.1406
4	0.0650	0.192	−0.1078
5	0.0581	0.181	−0.0942
6	0.0548	0.176	−0.0871
7	0.0532	0.174	−0.0833
8	0.0525	0.173	−0.0813
9	0.0523	0.173	−0.0803
10	0.0523	0.174	−0.0798
15	0.0537	0.179	−0.0809
∞	0.0637	0.206	−0.0962

and is 0.028% of the center deflection. Maximum deviation from zero normal slope occurs for the square and is 0.12% of the maximum slope within the plate. Comparing with results obtained when the problems are solved using only five equally spaced boundary points, we find maximum changes in $w(0, \theta)$, $M(0, \theta)$, and $M_x(a, 0)$ to be 0.006, 0.004, and 0.2%, respectively.

Significant results for the case when all sides are simply supported are presented in Table 2. The maximum deviation from zero deflection along the boundary is for the heptagon and is 0.15% of the center deflection. Maximum deviation from zero normal moment along the boundary occurs in the case of the hexagon and is 16.1% of the moment at the center. Although the moment deviation appears to be large, the residual moments along the edges oscillate to be essentially self-equilibrating and, by St. Venant's principle, should affect the moment at the center to a lesser extent. There is also more change in the results between solutions using five and nine boundary points for the simply supported case. The maximum changes in $w(0, \theta)$, $M(0, \theta)$, and $\partial w/\partial x(a, 0)$ are 2.4, 2.3, and 3.1%, respectively. For these reasons, the figures presented in Table 2 are given to fewer significant figures than those in Table 1.

To the authors' knowledge no other published results are available for comparison except for the triangular and square shapes. A partial summary of deflections and moments for these two cases is readily available in Ref. 2. The values in Tables 1 and 2 agree closely with those of Ref. 2 except for the value of bending moment at the center of a clamped triangular plate. Reference 2 presents differing values of M_x and M_y at $r = 0$, whereas, from considerations of symmetry and Mohr's circle, the bending moment at the center must be the same in all directions for any of the regular polygonal plate problems being presently considered.

Another result having interesting geometrical significance is that a mathematical maximum for bending moment occurs at the center for all shapes except the triangle. In the clamped case the mathematical maximum within the plate is $M_y = 0.1028\ q_0a^2$, occurring at $x = -0.210\ a$, $y = 0$ (see Fig. 1); in the simply supported case the maximum is $M_y = 0.233\ q_0a^2$, occurring at $x = -0.388\ a$, $y = 0$.

A final item of interest to be noted from Table 2 is that the deflection of simply supported, uniformly loaded regular polygonal plates is always less than that for their inscribing circles except for $m = 3$ and 4. This is because the conditions of zero tangential slope around the boundary of a polygonal plate result in it being clamped at its corners. Indeed the deflection steadily decreases as m increases from 3 to 10. Beyond $m = 10$, the effect of adding additional corners to the plate becomes overshadowed by the reduction in "clamping effectiveness" per corner because of the large interior angles present, and ultimately, as $m \to \infty$, the solution converges to that for the simply supported circle rather than the clamped one.

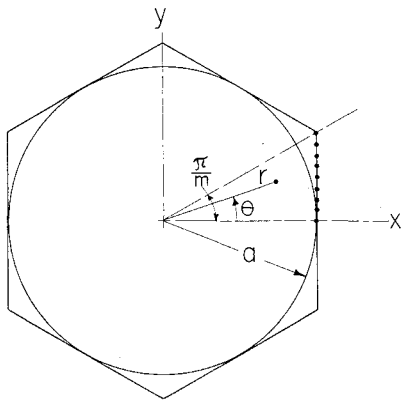

Fig. 1. Typical plate geometry.

References

[1] Niedenfuhr, F. W. and Leissa, A. W., "The torsion of prismatic bars of regular polygonal cross section," J. Aerospace Sci. **28**, 424–426 (1961).

[2] Timoshenko, S. and Woinowsky-Krieger, S., *Theory of Plates and Shells* (McGraw-Hill Book Co., Inc., New York, 1959).

Distributed Mass Matrix for Plate Element Bending

ROBERT J. GUYAN*
North American Aviation, Inc., Downey, Calif.

A METHOD of deriving distributed mass matrices for structural components has been given in Ref. 1. The method has been applied to the bending of beam elements in Ref. 1 and has been extended to include transverse shear and rotary inertia effects in Ref. 2.

The purpose of the present note is to provide the ingredients for forming a distributed mass matrix for plate element bending. Use of such a matrix in the natural mode analysis of plate and shell structures should significantly improve the accuracy of the results obtained using a diagonal mass matrix. Such improvements have already been demonstrated for beams.[1]

The kinetic energy of a plate element may be written

$$T = \frac{1}{2}\int_A m(x,y)\dot{d}^2 dA$$

where d represents the total displacement of the elemental area dA. In the Rayleigh-Ritz technique, the deformation of the system is represented by a set of unit displacement functions φ_i with amplitudes q_i. The expression for d is written

$$d(x,y,t) = \sum_i \varphi_i(x,y)\ q_i(t)$$

The q_i are the generalized displacements. For the plate there are 12 of these; the vertical deflection w and two coordinate slopes w_x and w_y at each of the four corners.

Substituting into T gives

$$T = \frac{1}{2}\sum_{i,j}\int_A m\varphi_i\varphi_j\dot{q}_i\dot{q}_j\ dA = \frac{1}{2}\sum_{i,j} m_{ij}\dot{q}_i\dot{q}_j$$

so that the elements of the mass matrix are determined from

$$m_{ij} = \int_A m(x,y)\varphi_i(x,y)\varphi_j(x,y)\ dA$$

To determine the φ_i, assume a form for the translation w. This may be written

$$w = \sum_i c_i\theta_i = c'\theta = \theta' c$$

The c_i are undetermined coefficients, and the θ_i are suitable polynomials. Although many choices for these are possible, only certain ones can be manipulated and also lead to satisfactory results. One such set is[3]: $\theta_1 = 1$, $\theta_2 = x$, $\theta_3 = y$, $\theta_4 = x^2/2$, $\theta_5 = xy$, $\theta_6 = y^2/2$, $\theta_7 = x^3/6$, $\theta_8 = x^2y/2$, $\theta_9 = xy^2/2$, $\theta_{10} = y^3/6$, $\theta_{11} = x^3y/6$, $\theta_{12} = xy^3/6$. With this expression for w, the generalized displacements may be written in the matrix form $q = \pi c$, where the elements of π are the coordinates of the four corners (Fig. 1) of the plate. Substituting back into the form for w after inversion of π gives $w = \theta'\pi^{-1}q$. The unit displacement functions φ_i are then determined as the translation w with $q_i = 1$ and all other generalized displacements equal to zero.

Received September 24, 1964.

* Research Specialist, Space and Information Systems Division. Member AIAA.